Evaluation of four global reanalysis products using in-situ observations in the Amundsen Sea Embayment, Antarctica

R. W. Jones[1], I. A. Renfrew[1], A. Orr[2],

B. G. M. Webber[1], D. M. Holland[3] and M. A. Lazzara[4]

[1]Centre of Ocean and Atmospheric Sciences, School of Environmental Science, University of East Anglia, Norwich, NR4 7TJ, UK.

[2]British Antarctic Survey, Cambridge, CB3 0ET, UK.

[3]Courant Institute of Mathematical Sciences, New York University, New York, NY, USA.

[4]Antarctic Meteorological Research Center, Space Science and Engineering Center, University of Wisconsin-Madison; and Department of Physical Sciences, School of Arts and Sciences Madison Area Technical College, Madison, Wisconsin, USA.

Corresponding author:

Mr. Richard Jones,

University of East Anglia, Norwich Research Park

Norwich, NR4 7TJ

Richard.W.Jones@uea.ac.uk

Key Points:

There are significant discrepancies in surface wind, humidity and temperature in the Amundsen Sea area.

Temperature biases greatest over and closer to the Antarctic continent and near the surface.

Validation data includes 38 radiosondes withheld from the reanalyses.

This article has been accepted for publication and undergone full peer review but has not been through the copyediting, typesetting, pagination and proofreading process which may lead to differences between this version and the Version of Record. Please cite this article as doi: 10.1002/2015JD024680

Abstract

The glaciers within the Amundsen Sea Embayment (ASE), West Antarctica, are amongst the most rapidly retreating in Antarctica. Meteorological reanalysis products are widely used to help understand and simulate the processes causing this retreat. Here we provide an evaluation against observations of four of the latest global reanalysis products within the ASE region – the ECMWF Interim Re-analysis (ERA-I), Japanese 55-year Reanalysis (JRA-55), Climate Forecast System Reanalysis (CFSR) and Modern Era Retrospective-Analysis for Research and Applications (MERRA). The observations comprise data from four automatic weather stations (AWS), three research-vessel cruises and a new set of 38 radiosondes all within the period 2009-2014.

All four reanalyses produce 2 m temperature fields that are colder than AWS observations, with the biases varying from approximately -1.8°C (ERA-I) to -6.8°C (MERRA). Over the Amundsen Sea, spatially averaged summertime biases are between -0.4°C (JRA-55) and -2.1°C (MERRA) with notably larger cold biases close to the continent (up to -6°C) in all reanalyses. All four reanalyses underestimate near surface wind speed at high wind speeds (>15 m s^{-1}) and exhibit dry biases and relatively large root-mean-square errors (RMSE) in specific humidity.

A comparison to the radiosonde soundings shows that the cold, dry bias at the surface extends into the lower troposphere; here ERA-I and CFSR reanalyses provide the most accurate profiles. The reanalyses generally contain larger temperature and humidity biases, (and RMSE) when a temperature inversion is observed; and contain larger wind speed biases (~2 to 3 m s^{-1}) when a low-level jet is observed.

1 Introduction

The glaciers within the Amundsen Sea Embayment (ASE; see Fig. 1a for location), one of the three major basins which drain the West Antarctic Ice Sheet, are amongst the most rapidly retreating in Antarctica; with this region responsible for about 10% of current global sea level rise [*Mouginot et al.,* 2014]. It is thought that this retreat is primarily driven by relatively warm circumpolar deep water being transported onto the continental shelf and driving basal melting of the ice shelves that buttress these glaciers [*Pritchard et al.,* 2012*; Rignot et al.,* 2013]. Ocean modelling and observations have revealed that large-scale zonal wind anomalies near the continental shelf break, are important in controlling the variability of this

melt [*Thoma et al.,* 2008*; Dutrieux et al.,* 2014]. Knowing the state of the atmosphere in the ASE over time is vital for understanding and modelling the climate processes at work here.

Meteorological reanalysis aim to provide the best estimate of the atmospheric state at any one time, by combining in-situ and satellite observations with forecast model data from a fixed version of a numerical weather prediction system. Usually reanalysis data sets provide global coverage over a period of several decades. As the ASE region is remote, and in-situ meteorological observations are sparse and unevenly distributed, reanalysis products are a valuable tool for studying weather and climate. However, because oceanographic and atmospheric models can be highly sensitive to their forcing data [*e.g. Condron and Renfrew, 2013*], it is necessary to evaluate reanalysis data against available in-situ measurements in order to determine their utility. Four of the latest generation of global reanalysis are evaluated here: the European Centre for Medium-Range Weather Forecasts (ECMWF) Interim Re-analysis (ERA-I), [*see Dee et al.,* 2011]; the Japanese 55-year Reanalysis (JRA-55), [*see Kobayashi et al.,* 2015]; the Climate Forecast System Reanalysis (CFSR) from the National Centre for Environmental Prediction (NCEP), [*see Saha et al.,* 2010] and the Modern Era Retrospective-Analysis for Research and Applications (MERRA) from National Aeronautics and Space Administration (NASA), [*see Rienecker et al.,* 2011].

Ocean models used to investigate the transport of circumpolar deep water onto the continental shelf in the Amundsen Sea have been driven by surface atmospheric forcing from a variety of different reanalysis products [*Thoma et al.,* 2008*; Schodlok et al.,* 2012*; Assmann et al.,* 2013*; Dutrieux et al.,* 2014]. Such modelling studies combined with oceanographic observations have increased scientific understanding of the processes causing the rapid retreat and thinning of glaciers such as Pine Island Glacier (PIG) [*Jacobs et al.,* 2011; *Assmann et al.,* 2013]. Weather and climate studies have also used reanalysis data: for example, to study seasonal cycles of the Amundsen Sea Low [*Hosking et al.*, 2013*; Turner et al.,* 2013] and atmospheric teleconnections between West Antarctic meteorological conditions and tropical ocean indices [*Ding et al.,* 2011*; Fogt et al.,* 2012*; Li et al., 2014; Clem and Fogt,* 2015], as well as forcing atmospheric models [*Deb et al., 2016*]. Glaciological studies such as *Medley et al.* [2014], have compared the average accumulation derived from a radar survey and firn cores with reanalysis data sets. This allows validation of their observation based accumulation rates and as such helps to constrain surface mass balance estimates.

Despite the frequent use of reanalysis products within the ASE, there has been, to our knowledge, no comprehensive effort to validate them in this data sparse region. *Bracegirdle* [2013] used pressure observations from three drifting buoys released in the neighbouring Bellingshausen Sea to evaluate mean-sea-level pressure fields from reanalysis products. The author found ERA-I had the smallest bias (~0.5 hPa), although both CFSR and MERRA also showed biases of less than 1 hPa. It has been shown that there are relatively large surface temperature biases over Antarctica in five global meteorological reanalysis data sets compared with automatic weather stations (AWS) both on the interior plateau and in outlying coastal regions – [*see Bracegirdle and Marshall,* 2012] and [*Jones and Lister,* 2015 (for ERA-I only)]. However neither of these studies included any observations from the coastal Amundsen Sea sector, nor from over the adjacent ocean.

Here we provide a comprehensive evaluation of ERA-I, MERRA, CFSR and JRA-55 for the ASE, including PIG. We use surface observations collected from four AWS and three research vessel cruises, as well as a new set of 38 radiosondes launched offshore during one of the oceanic cruises.

2 Data sets and methodology

2.1 Reanalyses

Four of the most recently released global reanalyses are evaluated in this study: ERA-I, JRA-55, CFSR and MERRA. For ERA-I, JRA-55 and MERRA the reanalysis fields are used, while for CFSR the near surface variables from the associated 6-hour re-forecast are used. (Note after 2010 CFSR version 2 data are used, this is essentially the same model as used in the first CFSR and version 2 is being used to extend the CFSR data forward to the present day; from here on we will refer to both products as the CFSR). The approximate grid size of the reanalysis products (at the tropics) is: ~79 km (T255) ERA-I , ~ 55km for JRA-55 (T319) , ~38km for CFSR (T382) and ~50km for MERRA (0.5° by 0.67°). ERA-I and JRA-55 both have 60 vertical levels with a model top at 0.1 hPa, CFSR has 64 vertical levels with the highest level at 0.26 hPa and MERRA has 72 vertical levels up to 0.01 hPa. All the reanalyses used here are provided at a 6 hour temporal resolution.

For evaluations such as this one, it is ideal to include some observational data sets which are *not* assimilated, i.e. that are entirely independent of the reanalysis data. Our radiosonde observations were definitely not assimilated as they were deliberately withheld from the Global Telecommunications System (GTS). The ECMWF website suggests that both sea-level pressure and wind speed from research vessels and all AWS data are made available via the GTS so could have been assimilated. In practice it is difficult to check whether every cruise or AWS data set has been assimilated.

2.2 Automatic weather stations

The Antarctic Meteorological Research Center (AMRC) has AWS observations from many sites around the continent. The Evans Knoll, Thurston Island and Bear Peninsula AWS's are all located in coastal areas of the ASE and henceforth we will refer to these as the AMRC sites (see Fig. 1b and Table 1 for locations). The AMRC AWS used here are of the CR1000 type, [*see Lazzara et al.*, 2012]. They were installed in January 2011 by scientists from New York University (NYU) and our evaluation period for these sites spans 1 February 2011 to 28 February 2014. We also use data from a fourth "NYU" AWS located on PIG, again installed by scientists from NYU and moved to its present location in January 2013. At this site the evaluation period spans 1 February 2013 to 28 February 2014. Each of the AWS records atmospheric temperature, relative humidity, wind speed and wind direction at a nominal height of 3 m above the surface, while atmospheric pressure is measured close to the foot of the mast (see Table 1 for average conditions; see Supplementary Table S1 for instrumentation details). The observations are stored at 10 minute temporal resolution, here we subsample the observations to 6 hourly temporal resolution for consistency with the reanalysis data.

All three of the AMRC sites are surrounded by complex topography, which is not fully resolved by the reanalyses. Such topography is typical for coastal regions of West Antarctica and the AWS sites are thus representative. The AMRC AWS were installed on nunataks (rock outcrops). The NYU AWS is located on PIG and the surrounding topography of the glacier is relatively uniform.

AWS in Antarctica are prone to overestimate temperature during low wind speed conditions due to a lack of ventilation [*Genthon et al.*, 2011; *Lazzara et al.*, 2012], particularly in austral summer when there is near 24 hour daylight. To mitigate this error, low wind speed periods (less than 2 m s^{-1}) are removed from the summertime temperature comparison (approximately 20% of the summertime data). Note at the Bear Peninsula AWS the anemometer stopped working during 2013 so the wind comparison there is based on only two years of data.

2.3 Research vessels

The research vessel meteorological data are from the *RRS James Clark Ross (JCR),* the *RV Polarstern* [*see König-Langlo,* 2010] and the *Nathaniel B. Palmer [see Jacobs,* 2014*]*. Observations of temperature, wind, humidity and pressure are used here (see Table S1 for details). Instruments on board the *JCR* were calibrated against national standards and we understand similar checks were carried out for the *Polarstern* and *Palmer* instruments. Each ship was within the ASE for approximately 1 month, the *JCR* in February-March 2014, the *Polarstern* in March 2010 and the *Palmer* in January-February 2009. Across the three research cruises there is approximately 3 months of data at 6 hourly resolution.

The sea-ice conditions differed somewhat between the three cruises. In 2009 when the *Palmer* was in the ASE the reanalysis products all show a high concentration of sea ice at the continental shelf break (see Fig. 1b for shelf-break location), extending to approximately 73°S and lower concentrations closer to PIG and Thwaites. In March 2010 while the *Polarstern* was in the region, there was a high concentration of sea ice to the west of the region shown in Fig. 1b (120°W and 110°W) but lower concentrations close to PIG and Thwaites Glacier. In February 2014 while the *JCR* was in the region, sea-ice concentrations were generally low but with an area of high concentration to the north of Thurston Island (see Fig. 1b for mean concentration).

2.4 Radiosondes

A set of 38 radiosondes were successfully launched between 1 February and 4 March 2014 during the *JCR* cruise (see Fig 1b for locations). The radiosondes were RS92 Våisålå sondes, measuring temperature, humidity and pressure with winds calculated using Global Positioning System (GPS). The RS92 Våisålå radiosondes have been shown to provide more accurate measurements of relative humidity at low temperatures than previous generation Våisålå sondes (RS90 and RS80) [*Suortti et al.*, 2008]. The variables are recorded every 2 seconds (~10 m intervals) during the ascent. Typically the radiosondes reached a maximum

altitude of approximately 20 km, well above the tropopause. Usually, there was one radiosonde launched each day at around 1200 UTC (see Table S2 for details). On three days (13, 18 and 23 February 2014) several sondes were launched to investigate particular weather events. The radiosonde profiles have been checked for consistency both with surface observations and within each profile and no calibration errors are found. In three of the profiles no wind data was recorded due to a problem with the GPS communications system. As noted above, these radiosonde observations were deliberately withheld from the GTS, and hence the reanalyses, in order to provide independent observations in the ASE.

2.5 Methodology

To allow comparison between the observations and gridded reanalysis data sets an appropriate methodology must be chosen. In the AWS comparison the nearest land grid point is used. For the ship and radiosonde data we use the nearest reanalysis grid point for the comparison. Due to the smoothed topography of the reanalyses, resulting in the seaward extension of the land sea mask in the ASE, a comparison to the nearest marine grid point is troublesome, as this can be ~100km distant. Instead we used the nearest grid point which does mean that on some occasions land grid points are used.

For the AWS data we focus our comparison on temperature, humidity, wind speed and wind direction. Reanalysis wind speed and direction are available at 10 m above the surface, and temperature and humidity fields at 2 m. In the AWS comparison, given the uncertainty of the observation height due to snow accumulation, the 2 m reanalysis fields are directly compared to the AWS temperature and humidity observations (recorded at a nominal height of 3 m above the surface). A height adjustment is applied to the 10-m reanalysis wind speed to 3 m, assuming a logarithmic wind profile with a roughness length of 0.1 mm (appropriate for snow) and neutral atmospheric stability – similar to [*Bromwich et al.,* 2013]. This simple adjustment is used as the atmospheric stability is unknown from the AWS observations.

It is also necessary to adjust the reanalysis temperatures for the difference in height between the grid point and the AWS. Failure to adjust temperatures in this way can result in spurious temperature biases [*Bracegirdle and Marshall, 2012*]. Due to the climatologically cold and dry Antarctic atmosphere, we adjusted the reanalysis temperatures to the listed altitude of each AWS using the dry adiabatic lapse rate of 9.8°C km^{-1}. The same 9.8°C km^{-1} adjustment was made by *Bracegirdle and Marshall* [2012], although *Jones and Lister* [2015] used the moist lapse rate of 6°C km^{-1}. Due to the presence of surface-based temperature inversions and

the often steep coastal topography, the lapse rate is likely to be highly variable, so the use of a constant lapse rate is an approximation. As an example of the size of this approximation, the height of the ERA-I gridpoint at Evans Knoll is 260m, 82m higher than the AWS height. Using the dry adiabatic lapse rate the ERA-I temperatures are adjusted by +0.8°C, whereas, if the 6°C km^{-1} lapse rate was used the adjustment would be +0.5°C. These differences are an order of magnitude smaller than the most significant biases discussed later. The AWS at Bear Peninsula, Thurston Island and on PIG (NYU) are co-located with UNAVCO GPS stations and as such we have some confidence in their listed elevation. However if the AWS altitudes are incorrectly listed, by e.g. 50 m, the temperature biases described later would change by ~0.5°C, the error in the listed elevation is unlikely to be larger than this. Table 1 shows the location and listed altitude of each AWS alongside the mean observed temperature and pressure.

The research vessel observations are recorded at heights between 19 and 37 m above the sea surface and are adjusted to 10 m or 2 m for comparison with the reanalysis products. In order to do this the observed sea surface and atmospheric temperatures are used to calculate atmospheric stability and then a height adjustment based on Monin-Obukhov similarity theory is made [*e.g. following, Smith,* 1988*; or Renfrew et al.,* 2002].

In the radiosonde comparison both the observations and reanalysis pressure-level data are interpolated on to a 5 hPa vertical grid. The focus here is on the lower troposphere so the comparison is limited to between the surface and 800 hPa (approximately 2 km altitude). Note also that the JRA-55 has a reduced horizontal resolution (1.5° by 1.5°) for its pressure-level data.

3 Results

3.1 Comparison with AWS observations

The representation of 2-m temperature is evaluated by season due to the large differences between summer and winter insolation in the Antarctic, which result in significant seasonal variations in temperature. During winter the absence of insolation allows longwave radiative cooling of the surface to dominate, generally resulting in the formation of a strongly stable, cold boundary layer [*King,* 1990]. In summer the boundary layer is warmer and tends to be weakly stably-stratified or even slightly unstable [*Mastrantonio et al.,* 1999].

As an example the seasonal temperature biases from the Bear Peninsula AWS are shown in Fig. 2. At Bear Peninsula (and across the other AMRC sites) ERA-I records its smallest bias

in the austral summer and its largest bias in the austral winter (Fig. 2). MERRA has large biases across all seasons (Fig. 2). Table 2 shows that across the AMRC sites both ERA-I and JRA-55 show a marked improvement in reproducing 2-m temperatures in summertime. Summertime biases for ERA-I and JRA-55 respectively are -0.23°C and -1.91°C, compared with -3.70°C (ERA-I) and -3.89°C (JRA-55) wintertime biases. This suggests that ERA-I and JRA-55 have more skill at capturing the weakly stable or even unstable summer boundary layer, whereas the CFSR and MERRA temperature biases show little seasonal variability.

Table 2 also shows that the mean 2-m temperature biases at the AMRC sites are negative during all seasons, for all the four reanalysis products. The weighted (by length of time series) mean annual bias for all four sites, shows that ERA-I has the smallest bias (-1.81°C), compared with CFSR (-2.50°C), JRA-55 (-2.62°C) and MERRA (-6.80°C). For MERRA the bias is significantly greater than the -1.6°C average bias found at coastal East Antarctic stations by *Bracegirdle and Marshall* [2012], suggesting MERRA may have a very strong regional bias in West Antarctica.

Jones and Lister [2015] using ERA-I show that 2-m temperatures are cold biased compared with a group of AWS on the Ross Sea coastline and three sites on the western side of the Antarctic Peninsula by between -1.1 and -2.4°C (for 2002-2013 period). Although at two sites on the Ross Sea (Cape Ross and Arelis) *Jones and Lister* [2015] find small positive biases for the same period. Here individual site biases range from -2.98°C at Thurston Island to +1.9°C at NYU, with three of the four sites showing cold biases of -1.5 to -3.0°C. These combined results, are suggestive of a systematic cold bias in ERA-I 2-m temperatures (of approximately -1.5°C) extending around West Antarctica from the Ross Sea to the Antarctic Peninsula.

The NYU AWS – located near the middle of the floating portion of PIG and at relatively low altitude – is notably different with positive biases in the ERA-I, JRA-55 and CFSR reanalyses (Table 2). The linear regression slope values are all less than 1 due to a warm bias at low temperatures (not shown). The NYU AWS is the only one located on an ice shelf and so may be more prevalent to cold-air drainage during katabatic flows – a phenomena that is difficult to properly model [*e.g. Renfrew*, 2004], leading to a warm bias. MERRA remains colder than observations at the NYU AWS, although the magnitude of the bias is smaller than that at the AMRC sites.

As an illustration of the summertime temperature comparisons, Fig. 3 shows scatter plots for the Bear Peninsula site which are representative of all the AMRC sites. The CFSR comparison (Fig. 3c) shows more scatter than the other products and consequently has a relatively large Root Mean Square Error (RMSE) and a reduced R^2 (correlation coefficient) value of 0.63, compared with 0.72 (MERRA), 0.74 (ERA-I) and 0.77 (JRA-55). Both CFSR and ERA-I tend to have larger RMSEs when observed summertime temperatures fall below -10°C. Furthermore, CFSR and MERRA tend to produce a larger range of summertime temperatures than observed, due to their anomalously cold temperatures, which leads to standard deviations that are larger than observed (Table 2). The bias in the MERRA comparison is noticeably larger than for the other reanalyses.

Wind speed and humidity comparison statistics can be found in Table 3. For brevity we show annual averages here as the seasonal differences are negligible. All of the reanalysis products are biased low in wind speed and struggle to reproduce the observed spread of wind speeds as indicated by standard deviation ratios of between 0.43 and 0.81. Figure 4 shows example scatter plots for the Thurston Island site, which is also representative of the other sites. The reanalyses tend to over-estimate the strength of the wind when the observed wind speed is low (< 5 m s^{-1}), and severely underestimate the strength of the wind when the observed wind speed is high (> 15 m s^{-1}). Across the AMRC sites the combination of these errors at low and high wind speeds causes the linear regression slopes to be very low, between 0.3 and 0.45 for all reanalysis products, compared to the ideal of 1 (Table 3 and Fig. 4). The performance at the NYU AWS site is similar, with all products showing a low slope and a negative bias. The reanalysis products represent low wind speeds better at NYU (not shown), leading to an improvement in the slope and correlation values there.

Analysis of strong wind events (> 15 m s^{-1}) at Thurston Island and Bear Peninsula revealed that at both sites the wind direction was from a north or north easterly direction during > 75% of these events (not shown). This suggests there may be an enhancement of the observed winds due to flow distortion, particularly at Thurston Island with mountainous terrain to the north (see Fig. 1b). Such flow distortion is poorly represented in models with insufficient resolution [*e.g. Renfrew et al., 2009; Elvidge et al, 2016*]. The northerly wind direction suggests that such winds are associated with synoptic-scale cyclones located offshore. Models with a coarser horizontal resolution have been shown to contain larger wind speed biases during Antarctic strong wind event where a cyclone and topographic effects combine to produce the strongest winds [*Turner et al., 2009; Orr et al., 2014]*.

The biases in the 2-m relative humidity (RH) field vary from -5.2% for ERA-I to 12.33% for CFSR (Table 3). RMSE range from 13% (JRA-55) to 17% (CFSR) at the AMRC sites. It is however notoriously difficult to measure RH particularly in the harsh environment in which these AWS are located, and problems with the observations may contribute to RH biases and RMSE [*Renfrew and Anderson,* 2002]. Due to the low observed temperatures the specific humidity is low, averaged across the AMRC sites the mean value is 1.42 g kg^{-1}. CFSR has the smallest dry bias in the specific humidity field of 0.05 g kg^{-1}. MERRA is drier than observed by 0.63 g kg^{-1}, ERA-I and JRA-55 produce dry biases of ~0.2 g kg^{-1}.

3.2 Comparison with research vessel observations

Summertime research vessel cruises to the Amundsen Sea have become frequent in recent years with several visits since 2007 [*Dutrieux et al.,* 2014]. Here we utilise research vessel meteorological data from three cruises (Table 4).

Pressure is extremely well represented by all the reanalyses; the magnitude of biases in mean-sea-level pressure are less than 0.5 hPa and the R^2 values are greater than 0.95 (Table 4). *Bracegirdle* [2013] found pressure biases of similar magnitude using drifting buoys in the neighbouring Bellingshausen Sea.

As seen in the AWS comparison, all four products show colder temperatures than those observed, with MERRA showing the largest average bias of -2.08°C. Similarly to the AWS comparison ERA-I and JRA-55 display a smaller (summertime) temperature bias than CFSR (Table 4). Figure 5 shows the spatial distribution of temperature biases for ERA-I and MERRA. In both products there is a tendency for temperature biases to be most negative closer to the coastline (with the largest biases approaching -6°C), this is also true of CFSR and JRA-55 (not shown). For MERRA the negative temperature bias is particularly clear in the *JCR* and *Palmer* comparisons as these cruises spent more time close to PIG ice shelf. The temperature biases for the AWS sites corroborate the research vessel comparison, as illustrated in Fig. 5 (top row).

The reanalysis products underestimate the mean wind speed compared to the ship observations by between -0.32 m s^{-1} (JRA-55) and -1.02 m s^{-1} (MERRA). There is no clear pattern of spatial variability in the wind speed bias for any of the reanalysis products, as illustrated for JRA-55 in Fig. 6. Scatter plots for all three cruises (not shown) indicate an improved representation of high wind speeds than was seen in the AWS comparison. The biases even at wind speeds between 15 and 19 m s^{-1} (the highest observed ship wind speeds)

are small. Pressure and wind speed observations from the research vessels are made available for assimilation into the reanalyses and this may be partly why the bias is reduced. In contrast to the results seen here, *Li et al.* [2013] have shown that ERA-I contains biases at low and high wind speeds compared with Southern Ocean ship observations, overestimating low winds and underestimating high winds. Here we see little evidence of such systematic biases but note that our sample is limited, there are few strong wind observations from the research vessels in the Amundsen Sea.

Biases in the specific and relative humidity fields are generally slightly smaller than those seen in a comparison to summertime AWS observations (not shown). The spatial distribution of biases (not shown) reveals that there is a tendency for larger dry biases in the specific humidity fields of MERRA and CFSR close to the coastline. This is spatially coherent with low temperature biases observed in the same region (see Fig. 5). As MERRA and CFSR both give temperatures that are too cold they are also likely to have too little moisture. In the other reanalysis products there are no clear spatial patterns in the humidity biases; large biases are seen in many different locations for relative humidity in particular.

3.3 Comparison with radiosonde data

A set of 38 radiosondes was launched in the Amundsen Sea from the *JCR* cruise during February and March 2014. Having been deliberately withheld from the reanalyses they provide a unique observational data set for validating reanalysis products in this region. Here we focus on a comparison between 975 and 800 hPa, as the lower troposphere is most important for the underlying ocean and glaciers.

All of the reanalysis products have a mean temperature profile colder than the radiosondes; the 975-800 hPa mean temperature bias varies between -0.54°C for ERA-I and -1.22°C for JRA-55 (Table 5). This cold bias is consistent in sign with the research vessel near-surface temperature biases (e.g. Fig. 5). The mean temperature profiles in Fig. 7a show that CFSR and ERA-I mean temperatures are accurate to within ~1°C of the average radiosonde temperature from 975 hPa to 800 hPa. JRA-55 also produces a similar shaped mean profile compared with the observations, but has a larger bias of between -1 and -2°C. In the boundary layer MERRA has a large cold bias: at 975 hPa the average MERRA temperature is 4°C colder than the observations, consistent with the large near-surface biases observed during the *JCR* cruise (Fig. 5; Table 4).

All four of the reanalyses produce similar mean wind speed profiles (Fig. 7c). At 975 hPa they all accurately reproduce near-surface wind speed to within 1 m s^{-1}. Above this the observations show a distinct low-level jet (discussed later) which is not captured by the reanalyses. As such there is a negative bias for all of the products, with average wind speeds ~2 m s^{-1} lower than the observations between 950-850 hPa.

The specific (Fig. 7b) and relative humidity (Fig. 7d) mean profiles reveal that ERA-I and CFSR provide accurate profiles of atmospheric moisture; ERA-I is perhaps the most accurate, particularly in the relative humidity profile. MERRA and JRA-55 are both drier than the observations, although JRA-55 accurately produces the relative humidity profile between 975 and 920 hPa, with larger biases above this. The specific humidity profile shows a significant dry bias of 0.5 g kg^{-1} for MERRA between 975 hPa and 925 hPa, which reduces with increasing height. This is linked to the MERRA cold bias, colder air can hold less moisture, and as such there is a dry bias in the same part of the profile as the cold bias. *Jakobson et al.* [2012] also find that MERRA is drier than observations of both specific and relative humidity in the Arctic, which suggests that MERRA may have difficulties with moisture budgets or transport near Arctic sea ice and continental shelf regions of Antarctica.

By splitting the radiosondes into two groups by location (see Fig. 1b) it becomes clear that the temperature biases seen in Fig. 7 are, in the main, caused by the group of radiosondes launched closer to the Antarctic continent (Fig. 8; Table 5). All of the reanalyses have a much larger mean temperature bias for the 'continental' profiles than for the 'shelf break' radiosondes, with JRA-55 and MERRA producing the largest mean (975-800 hPa) biases of -1.60°C and -1.50°C respectively. For MERRA the negative temperature bias between 975-900 hPa only occurs for the 'continental' profiles, consistent with the distribution of surface biases in comparison with ship observations (Fig. 5). In the layer between 975 hPa and 940 hPa, the lowest few hundred metres of the atmosphere, the MERRA mean temperature in the continental group is 4.23°C colder than that of the radiosondes.

The wind speed profiles have also been split into two distinct groups: those containing a low-level jet (LLJ) and those without (Fig. 9). A LLJ in its most simplistic form is a wind speed maximum in the lower part of the atmosphere. In order to identify LLJs the definition from *Stull* [1988], and later modified by *Andreas* [2000], is used. Namely, to be classified as a LLJ a wind speed maxima must occur in the lowest 1.5 km of the atmosphere and must be at least 2 m s^{-1} faster than both the wind speed minimum above it and the wind speed recorded at the surface. LLJs were observed in 21 of the 38 radiosonde soundings (see Fig. 1b for locations).

Fig. 9 shows that in the group of soundings where an LLJ is *not* observed all the reanalysis products accurately simulate the wind speed profile between 975 and 900 hPa. Above this they tend to underestimate wind speed by between 1 and 2 m s^{-1}. When there is a LLJ, the reanalysis products (on average) show positive wind shear between 975 and 925 hPa, which indicates that at least some of the LLJs are being captured. However they all underestimate the jet wind speed by ~2 m s^{-1}, which indicates they are either failing to produce the maximum wind speed within the LLJs or they underestimate the frequency of LLJs; inspection of individual profiles reveals that both are factors. In comparison to Arctic dropsonde data it has been shown that ERA-I tends to produce LLJs that are both too broad and too weak [*Liu et al.,* 2015]. The mean profiles in *Liu et al.* [2015] are similar to those seen here, with ERA-I managing to reproduce wind speed maxima at approximately the same altitude as the observations but unable to reproduce the magnitudes observed. Normalised bias profiles (not shown) indicate that the bias relative to the mean observed wind speed is greater in the LLJ group than in the non-LLJ group, i.e. the reanalyses perform worse when there is a LLJ.

The radiosonde profiles have also been split on the basis of whether or not they contain a low-level temperature inversion (see Table 5). Here a temperature inversion is defined as a temperature increase of > 2°C (between the base and top of the inversion) within the profile between 975 and 800 hPa. The JRA-55, CFSR and MERRA reanalyses all have significantly larger biases in the group of profiles when there is a temperature inversion. This larger bias is particularly apparent in the layer between 975 and 875 hPa where almost all of the temperature inversions were observed (not shown). Given that the vertical depth of temperature inversions in the observations is typically hundreds of metres, the coarse vertical resolution of reanalysis products will struggle to capture this feature. ERA-I has a similar magnitude temperature bias in both groups, although larger RMSE in the inversion group. In the inversion group both MERRA and JRA-55 also contain larger specific humidity biases, while MERRA also has a larger RH bias (Table 5). For MERRA it seems that the additional bias is driven by a larger dry bias between 975 and 900 hPa. However in JRA-55 the increased bias is due to the layer between 900 and 800 hPa, which is typically above the height of temperature inversions. In the Arctic multiple studies have found similar problems with the strength and depth of temperature inversions in reanalysis products [*Lüpkes et al.,* 2010*; Pavelsky et al.,* 2010*; Harden et al.,* 2011*; Jakobson et al.,* 2012]. *Lüpkes et al.* [2010] show that ERA-I overestimates the altitude of the inversion base. Here individual profiles

(not shown) suggest that reanalysis inversions are vertically too broad and often too weak, contributing to the larger temperature biases seen in JRA-55, CFSR and MERRA.

4 Discussion

4.1 Common reanalysis traits

All four of the reanalyses generally produce lower temperatures than those observed at the AWS sites. This cold bias is also evident (to a lesser extent) over the open ocean in the comparison with summertime observations from research vessels and radiosondes. Over the ocean all of the products display greater cold biases near to the coastline compared with further out to sea, in agreement with temperature profile comparisons to the radiosondes. All the reanalyses are generally less accurate for temperature and humidity profiles closer to the continent and when there is a low-level inversion.

The AWS comparison revealed that all of the reanalysis products underestimate strong wind events (> 15 m s^{-1}), suggesting they struggle to capture orographic and katabatic enhancement of the winds, and they overestimate low wind speeds. The reanalyses provide an improved representation of wind speeds over the ocean, when compared with the summertime research vessel observations. They continue to show small negative biases in mean wind speed but the systematic biases at low and high wind speeds are not seen. The reanalyses are generally less accurate for wind speed profiles when a LLJ occurs; these are typically underestimated by 2-3 m s^{-1}. This is consistent with *Liu et al.* [2015] where ERA-I produced LLJs that were too weak and too vertically diffuse in comparison with Arctic dropsonde data.

4.2 ERA-I specifics

Compared with observations at the three AMRC AWS (with three year records), ERA-I shows the smallest cold biases of between -1.4°C and -3.0°C. These biases are similar to those found by *Jones and Lister* [2015] at AWS sites around the Ross Sea coastline, but they are larger than the ERA-I cold biases in coastal East Antarctica found by *Bracegirdle and Marshall* [*2012*]. ERA-I has a much larger cold bias in austral winter than summer, possibly because it is not accurately reproducing the strong surface-based inversion that is commonly observed during the polar night [*King,* 1990]. Generally ERA-I has the smallest cold bias of the reanalyses examined, although JRA-55 performs slightly better in the research-vessel comparison.

Relative and specific humidity biases in ERA-I are small compared with the other reanalysis products. Across the three comparisons specific humidity biases are between -0.05 and -0.20 g kg^{-1}, while RH biases are between -1 and -6%, although the RMSE for RH are generally between 5 and 15%.The wind speed biases are typically between -0.80 and -1.40 m s^{-1} (only JRA-55 has smaller wind speed biases) and the pattern of the biases at high and low wind speeds compared with AWS observations is the same as that seen in the other reanalyses. Overall, ERA-I contains the smallest temperature and humidity biases compared with observational data sets in the ASE, making it the most accurate product, based on this comparison.

4.3 JRA-55 specifics

JRA-55 cold biases are somewhat larger than those seen in ERA-I but typically smaller than those in CFSR and MERRA, particularly in the comparison with research vessel data. In the shelf break group of radiosonde profiles, and from the research vessel comparison, JRA-55 produces similar statistics to ERA-I for temperature over open water. JRA-55 contains the smallest biases in wind speed compared to AWS and research vessel observations. Generally, in the research vessel comparison JRA-55 is the most accurate of the reanalysis products, however in the radiosonde profile comparisons it produces temperature and wind speed profiles with larger biases and RMSEs than ERA-I. This may be in part due to the reduced horizontal resolution of its pressure level data. Overall JRA-55 compares well to the in-situ observations.

4.4 CFSR specifics

Compared with AWS observations the magnitude of CFSR cold biases are relatively constant across all four seasons but larger than those seen in ERA-I and JRA-55 (e.g. Table 2; Fig. 2). Fig. 3c shows that in summertime the CFSR cold bias is larger when the observed temperature is lower. Generally, the CFSR cold biases in the ASE are larger than those found in coastal East Antarctica by *Bracegirdle and Marshall* [2012]. Radiosonde cold biases are slightly larger than ERA-I, but smaller than JRA-55 and MERRA. The CFSR humidity profiles are as accurate as ERA-I, producing the correct shape of both relative and specific humidity profiles. The specific humidity biases are also typically small between -0.02 and -0.22 g kg^{-1} across the three comparisons, similar to values from ERA-I. The CFSR wind speed comparison against the AWS has the largest negative bias, although the performance over the ocean is comparable to the other reanalyses.

4.5 MERRA specifics

MERRA has the largest temperature bias of the four reanalysis products evaluated. Near surface temperatures are colder than the AWS observations by approximately 6.8°C. This is significantly larger than the MERRA cold biases found by *Bracegirdle and Marshall* [2012] in coastal East Antarctica, which implies this large cold bias may be confined to West Antarctica. Fig. 5 demonstrates that MERRA temperature biases are much larger close to the continent – a spatial pattern that is enhanced compared to the other reanalyses. Profiles suggest MERRA predicts a surface-based temperature inversion that is both stronger and more frequent than seen in the observations.

Specific humidity biases are also larger than in the other reanalysis products, with dry biases of 0.5 g kg^{-1} for the radiosonde and AWS comparisons. *Jakobson et al.* [2012] find MERRA had a similar magnitude dry bias in the lower troposphere over the Arctic, but there the magnitude of the bias increased with height rather than decreased. Overall, large temperature and humidity biases make MERRA the least accurate of the reanalysis products for the Amundsen Sea.

4.6 Implications

Overall, the reanalyses assessed here provide a reasonable estimate of the state of the atmosphere over the ASE. But while their accuracy at moderate wind speeds over open water is good, there should be some caution when wind speeds are high (> 15 m s^{-1}), as these high wind speeds are likely to be underestimated, and near complex coastal topography where the reanalyses are unable to adequately capture the variability in winds. For example, the research vessel (and radiosonde) RMSE are relatively large compared to other open-ocean locations [*e.g. Li et al.*, 2013; *Harden et al*., 2015]. These shortcomings would lead to underestimates in surface wind stress during high wind speed conditions and consequently alter the wind stress curl. Errors in the wind stress and its curl would lead to errors in the dynamics of an ocean model forced by these reanalyses, and will hamper the interpretation of observed ocean variability. They could also lead to an under-estimate of sea-ice divergence and the frequency of coastal polynyas.

The cold bias will affect both the surface sensible and latent heat fluxes, implying an overestimate in both heat fluxes (as the reanalyses are too cold and too dry). It has previously been shown that an older reanalysis product, the National Centre for Environmental Prediction Reanalysis 1, contained a cold temperature bias which changed the modelled melt rates of ice shelves and ice shelf cavities in the Amundsen Sea [*Timmermann et al.,* 2012; *Nakayama et al.,* 2014]. However, the cold (and dry) bias combined with the potential underestimation of high wind speeds may partially offset one another for the heat fluxes [*e.g. Renfrew et al.,* 2002]. Nevertheless, such errors cannot entirely compensate across a range of values, so unknown errors will be introduced. In addition, the spatial distribution of these biases may lead to an underestimation of the importance of surface fluxes near the coast where the cold biases are particularly large.

5. Conclusions

In a validation study for the Amundsen Sea Embayment, the four most recently released global meteorological reanalysis products all produce cold biases of between approximately -1.8°C (ERA-I) and -6.8°C (MERRA) when compared with year-round AWS observations. Cold biases were also found in comparisons with ship-based and radiosonde observations, although these comparisons are restricted to the summer lower-troposphere. ERA-I has the smallest temperature bias. The reanalysis cold bias in coastal regions of Antarctica is in agreement with previous studies [*Bracegirdle and Marshall,* 2012*; Jones and Lister,* 2015], although these did not cover coastal West Antarctica. A seasonal comparison of the biases shows that ERA-I has the smallest temperature bias in austral summer but all reanalysis products contain cold biases in austral winter. This implies parameterizations may perform less well during the winter months. For all the reanalysis products the magnitude of temperature biases varies spatially. Close to the ice shelves that form large parts of the ASE coastline, the cold bias is much larger than in areas more distant from the coastline. Vertical profiles from the reanalyses generally correspond better away from the coastline and in the absence of temperature inversions or low-level jets.

In the comparison to AWS wind speeds, all four reanalysis products severely underestimate when observations are above 15 m s^{-1} and overestimate when observations are below 5 m s^{-1}. Over the ocean, compared with research vessel observations, the reanalyses provide improved representation of wind speed. This is in contrast with results from *Li et al.* [2013] who found ERA-I contained the same low and high wind biases in a comparison with Southern Ocean ship observations.

Overall, ERA-I has the smallest biases and errors in near-surface fields compared with meteorological observations within the ASE. This is consistent with the Antarctic-wide study of *Bracegirdle and Marshall* [2012]. CFSR and JRA-55 have slightly larger cold biases but have a similar level of accuracy as ERA-I in the wind speed and humidity fields. MERRA contains the largest surface temperature bias and because of this also contains a large dry bias. The large MERRA temperature bias may be spatially limited to ASE (c.f. *Bracegirdle and Marshall* [2012]). The biases at high and low observed wind speeds may be indicative of winds around other parts of coastal Antarctica.

Despite the use of a wide variety of meteorological data sets in this study there remains a lack of observations from West Antarctica. For example, the authors are not aware of any sustained wintertime meteorological observations over the sea ice or open water of the Amundsen Sea. Through fully utilising the existing observations and introducing a new data set this study provides a generally consistent evaluation of the reanalysis products in this area.

Acknowledgements

The authors appreciate the support of the University of Wisconsin-Madison Automatic Weather Station Program (via http://amrc.ssec.wisc.edu) for the data set, data display, and information, NSF grant numbers ANT-0944018 and ANT-1245663. Further thanks to the support team at NYU for the pre-processing and provision of data from the AWS installed on PIG, all made possible by NSF grant ANT‐0732869 and NYU Abu Dhabi G1204. The *JCR* meteorological data and radiosonde observations will become available from the British Oceanographic Data Centre during 2016 https://www.bodc.ac.uk. For further information or immediate access to the radiosonde data contact the corresponding author. The *Polarstern* meteorological data are available from the PANGAEA website http://doi.pangaea.de/10.1594/PANGAEA.743575. The *Palmer* meteorological data are available from http://www.marine-geo.org/tools/search/Files.php?data_set_uid=9878. The authors would also like to thank the staff at the Computational and Information Systems Laboratory research data archive for providing access to the reanalysis data sets for ERA-Interim, CFSR and JRA-55 (via http://rda.ucar.edu). The Global Modeling and Assimilation Office (GMAO) and the GES DISC are acknowledged for the dissemination of the MERRA dataset (via http://disc.sci.gsfc.nasa.gov).

This work was supported by funding from the UK Natural Environment Research Council's iSTAR Programme and NERC grant number (NE/J005703/1), through a NERC funded PhD (NE/K011154/1) based at the University of East Anglia. Many thanks to iSTAR colleagues for their helpful advice and comments on this work, particularly to all science staff and crew on board *JCR 294/295* for their assistance with launching radiosondes.

The authors wish to thank the reviewers for their helpful comments and suggestions which have improved this manuscript.

References

Andreas, E., Claffy, K., & Makshtas, A. (2000). Low-level atmospheric jets and inversions over the western Weddell Sea. *Boundary-Layer Meteorology*, 459–486.

Assmann, K. M., Jenkins, A., Shoosmith, D. R., Walker, D. P., Jacobs, S. S., & Nicholls, K. W. (2013). Variability of Circumpolar Deep Water transport onto the Amundsen Sea Continental shelf through a shelf break trough. *Journal of Geophysical Research: Oceans*, *118*(12), 6603–6620. http://doi.org/10.1002/2013JC008871

Bracegirdle, T. J. (2013). Climatology and recent increase of westerly winds over the Amundsen Sea derived from six reanalyses. *International Journal of Climatology*, *33*(4), 843–851. http://doi.org/10.1002/joc.3473

Bracegirdle, T. J., & Marshall, G. J. (2012). The Reliability of Antarctic Tropospheric Pressure and Temperature in the Latest Global Reanalyses. *Journal of Climate*, *25*(20), 7138–7146. http://doi.org/10.1175/JCLI-D-11-00685.1

Bromwich, D. H., Otieno, F. O., Hines, K. M., Manning, K. W., & Shilo, E. (2013). Comprehensive evaluation of polar weather research and forecasting model performance in the Antarctic. *Journal of Geophysical Research: Atmospheres*, *118*(2), 274–292. http://doi.org/10.1029/2012JD018139

Clem, K., & Fogt, R. (2015). South Pacific circulation changes and their connection to the tropics and regional Antarctic warming in austral spring, 1979–2012. *Journal of Geophysical Research: Atmospheres*, *120*, 2773–2792. http://doi.org/10.1002/2014JD022940.

Condron, A. and Renfrew, I. A. (2013). The impact of polar mesoscale storms on northeast Atlantic Ocean circulation, *Nature Geoscience*, **6,** 34-37. doi:10.1038/ngeo1661

Deb, P., Orr, A., Hosking, S. H., Phillips, T., Turner, J., Bannister D., Pope, J., and Colwell, S. (2016). An assessment of the Polar Weather Research and Forecast (WRF) model representation of near-surface meteorological variables over West Antarctica. *Journal of Geophysical Research - Atmospheres*. 10.1002/2015JD024037

Dee, D. P., Uppala, S. M., Simmons, A. J., Berrisford, P., Poli, P., Kobayashi, S., Andrae, U., Balmaseda, M. A., Balsamo, G., Bauer, P., Bechtold, P., Beljaars, A. C. M., van de

Berg, L., Bidlot, J., Bormann, N., Delsol, C., Dragani, R., Fuentes, M., Geer, A. J., Haimberger, L., Healy, S. B., Hersbach, H., Hólm, E., V. Isaksen, L., Kållberg, P., Köhler, M., Matricardi, M., McNally, A. P., Monge-Sanz, B. M., Morcrette, J.-J., Park, B.-K., Peubey, C., de Rosnay, P., Tavolato, C., Thépaut, J.-N., & Vitart, F. (2011). The ERA-Interim reanalysis: configuration and performance of the data assimilation system. *Quarterly Journal of the Royal Meteorological Society*, *137*(656), 553–597. http://doi.org/10.1002/qj.828

Ding, Q., Steig, E. J., Battisti, D. S., & Küttel, M. (2011). Winter warming in West Antarctica caused by central tropical Pacific warming. *Nature Geoscience*, *4*(6), 398–403. http://doi.org/10.1038/ngeo1129

Dutrieux, P., De Rydt, J., Jenkins, A., Holland, P. R., Ha, H. K., Lee, S. H., Steig, E. J., Ding, Q., Abrahamsen, P. E., & Schröder, M. (2014). Strong sensitivity of Pine Island ice-shelf melting to climatic variability. *Science (New York, N.Y.)*, *343*(6167), 174–8. http://doi.org/10.1126/science.1244341

Elvidge, A. D., Renfrew, I. A., King, J. C., Orr, A., Lachlan-Cope, T. A. (2016). Foehn warming distributions in non-linear and linear flow regimes: A focus on the Antarctic Peninsula, *Quarterly J. Royal Meteorol. Soc.*, **142,** 618-631. doi:10.1002/qj.2489

Fogt, R. L., Wovrosh, A. J., Langen, R. A., & Simmonds, I. (2012). The characteristic variability and connection to the underlying synoptic activity of the Amundsen-Bellingshausen Seas Low. *Journal of Geophysical Research: Atmospheres*, *117*(D7), http://doi.org/10.1029/2011JD017337

Genthon, C., Six, D., Favier, V., Lazzara, M., & Keller, L. (2011). Atmospheric Temperature Measurement Biases on the Antarctic Plateau. *Journal of Atmospheric and Oceanic Technology*, *28*(12), 1598–1605. http://doi.org/10.1175/JTECH-D-11-00095.1

Harden, B. E., Renfrew, I. A., & Petersen, G. N. (2011). A Climatology of Wintertime Barrier Winds off Southeast Greenland. *Journal of Climate*, *24*(17), 4701–4717. http://doi.org/10.1175/2011JCLI4113.1

Harden, B. E., I. A. Renfrew and Petersen, G. N. (2015). Meteorological buoy observations from the central Iceland Sea, *Journal of Geophysical Research: Atmospheres,* **120,** doi:10.1002/2014JD022584.

Hosking, J. S., Orr, A., Marshall, G. J., Turner, J., & Phillips, T. (2013). The influence of the Amundsen-Bellingshausen Seas Low on the climate of West Antarctica and its representation in coupled climate model simulations. *Journal of Climate*, *26*(17), 130315144221005. http://doi.org/10.1175/JCLI-D-12-00813.1

Jacobs, S. S., Jenkins, A., Giulivi, C. F., & Dutrieux, P. (2011). Stronger ocean circulation and increased melting under Pine Island Glacier ice shelf. *Nature Geoscience*, *4*(8), 519–523. http://doi.org/10.1038/ngeo1188

Jacobs, S.S. (2014). Underway Hydrographic, Weather and Ship-state Data (JGOFS) from Nathaniel B. Palmer expedition NBP0901 (2009). *Integrated Earth Data Applications (IEDA)*. http://dx.doi.org/10.1594/IEDA/309878.

Jakobson, E., Vihma, T., Palo, T., Jakobson, L., Keernik, H., & Jaagus, J. (2012). Validation of atmospheric reanalyses over the central Arctic Ocean. *Geophysical Research Letters*, *39*(10). http://doi.org/10.1029/2012GL051591

Jones, P. D., & Lister, D. H. (2015). Antarctic near-surface air temperatures compared with ERA-Interim values since 1979. *International Journal of Climatology*, *35*(7), 1354–1366. http://doi.org/10.1002/joc.4061

King, J. C. (1990). Some measurements of turbulence over an antarctic ice shelf. *Quarterly Journal of the Royal Meteorological Society*, *116*(492), 379–400.

Kobayashi, S., Ota, Y., Harada, Y., Ebita, A., Moriya, M., Onoda, H., Onogi, K., Kamahori, H., Kobayashi, C., Endo, H., Miyaoka, K., & Takahashi, K. (2015). The JRA-55 Reanalysis: General Specifications and Basic Characteristics. *Journal of the Meteorological Society of Japan. Ser. II*, *93*(1), 5–48. http://doi.org/10.2151/jmsj.2015-001

König-Langlo, G. (2010): Continuous meteorological surface measurement during POLARSTERN cruise ANT-XXVI/3. *Alfred Wegener Institute, Helmholtz Center for Polar and Marine Research, Bremerhaven*, doi:10.1594/PANGAEA.743575

Lazzara, M. A., Weidner, G. A., Keller, L. M., Thom, J. E., & Cassano, J. J. (2012). Antarctic Automatic Weather Station Program: 30 Years of Polar Observation. *Bulletin of the American Meteorological Society*, *93*(10), 1519–1537. http://doi.org/10.1175/BAMS-D-11-00015.1

Li, M., Liu, J., Wang, Z., Wang, H., Zhang, Z., Zhang, L., & Yang, Q. (2013). Assessment of Sea Surface Wind from NWP Reanalyses and Satellites in the Southern Ocean. *Journal of Atmospheric and Oceanic Technology*, *30*(8), 1842–1853. http://doi.org/10.1175/JTECH-D-12-00240.1

Li, X., Holland, D. M., Gerber, E. P., & Yoo, C. (2014). Impacts of the north and tropical Atlantic Ocean on the Antarctic Peninsula and sea ice. *Nature, 505(7484)*, 538-542.

Liu, Z., Schweiger, A., & Lindsay, R. (2015). Observations and Modeling of Atmospheric Profiles in the Arctic Seasonal Ice Zone. *Monthly Weather Review*, *143*(1), 39–53. http://doi.org/10.1175/MWR-D-14-00118.1

Lüpkes, C., Vihma, T., Jakobson, E., König-Langlo, G., & Tetzlaff, A. (2010). Meteorological observations from ship cruises during summer to the central Arctic: A comparison with reanalysis data. *Geophysical Research Letters*, *37*(9) L09810. http://doi.org/10.1029/2010GL042724

Mastrantonio, G., Malvestuto, V., Argentini, S., Georgiadis, T., & Viola, A. (1999). Evidence of a Convective Boundary Layer Developing on the Antarctic Plateau during the Summer. *Meteorology and Atmospheric Physics*, *71*(1-2), 127–132.

Medley, B., Joughin, I., Smith, B. E., Das, S. B., Steig, E. J., Conway, H., Gogineni, S., Lewis, C., Criscitiello, A. S., McConnell, J. R., van den Broeke, M. R., Lenaerts, J. T. M., Bromwich, D. H., Nicolas, J. P., Leuschen, C. (2014). Constraining the recent mass

balance of Pine Island and Thwaites glaciers, West Antarctica, with airborne observations of snow accumulation. *The Cryosphere*, *8*(4), 1375–1392. http://doi.org/10.5194/tc-8-1375-2014

Mouginot, J., Rignot, E., & Scheuchl, B. (2014). Sustained increase in ice discharge from the Amundsen Sea Embayment, West Antarctica, from 1973 to 2013. *Geophysical Research Letters*, *41*(5), 1576–1584. http://doi.org/10.1002/2013GL059069

Nakayama, Y., Timmermann, R., Schröder, M., & Hellmer, H. H. (2014). On the difficulty of modeling Circumpolar Deep Water intrusions onto the Amundsen Sea continental shelf. *Ocean Modelling*, *84*, 26–34. http://doi.org/10.1016/j.ocemod.2014.09.007

Orr, A., Phillips, T., Webster, S., Elvidge, A., Weeks, M., Hosking, S., Turner, J. (2014). Met Office Unified Model high resolution simulations of a strong wind event in Antarctica. *Quarterly Journal of the Royal Meteorological Society. 140(684), 2287-2297.* http://doi.org/10.1002/qj.2296

Pavelsky, T. M., Boé, J., Hall, A., & Fetzer, E. J. (2010). Atmospheric inversion strength over polar oceans in winter regulated by sea ice. *Climate Dynamics*, *36*(5-6), 945–955. http://doi.org/10.1007/s00382-010-0756-8

Pritchard, H. D., Ligtenberg, S. R. M., Fricker, H. A, Vaughan, D. G., van den Broeke, M. R., & Padman, L. (2012). Antarctic ice-sheet loss driven by basal melting of ice shelves. *Nature*, *484*(7395), 502–5. http://doi.org/10.1038/nature10968

Renfrew, I. A. (2004). The dynamics of idealized katabatic flow over a moderate slope and ice shelf. *Quarterly Journal of the Royal Meteorological Society*, *130*(598), 1023–1045. http://doi.org/10.1256/qj.03.24

Renfrew, I. A., & Anderson, P. (2002). The surface climatology of an ordinary katabatic wind regime in Coats Land, Antarctica. *Tellus A*, 463–484.

Renfrew, I. A., Moore, G.W.K., Guest, P.S., and Bumke, K. (2002). A comparison of surface layer and surface turbulent flux observations over the Labrador Sea with ECMWF analyses and NCEP reanalyses. *Journal of Physical Ocenography*, 32(2), 383–400.

Renfrew, I.A.,Petersen, G. N., Sproson, D. A. J., Moore, G.W.K., Adiwidjaja, H., Zhang, S., and North, R. (2009). A comparison of aircraft-based surface-layer observations over Denmark Strait and the Irminger Sea with meteorological analyses and QuikSCAT winds, *Quarterly J. Royal Meteorol. Soc.*, **135,** 2046-2066.

Rienecker, M. M., Suarez, M. J., Gelaro, R., Todling, R., Bacmeister, J., Liu, E., Bosilovich, M. G., Schubert, S. D., Takacs, L., Kim, G-K., Bloom, S., Chen, J., Collins, D., Conaty, A., da Silva, A., Gu, W., Joiner, J., Koster, R. D., Lucchesi, R., Molod, A., Owens, T., Pawson, S., Pegion, P., Redder, C. R., Reichle, R., Robertson, F. R., Ruddick, A. G., Sienkiewicz, M., & Woollen, J. (2011). MERRA: NASA's Modern-Era Retrospective Analysis for Research and Applications. *Journal of Climate*, *24*(14), 3624–3648. http://doi.org/10.1175/JCLI-D-11-00015.1

Rignot, E., Jacobs, S., Mouginot, J., & Scheuchl, B. (2013). Ice-shelf melting around Antarctica. *Science (New York, N.Y.)*, *341*(6143), 266–70. http://doi.org/10.1126/science.1235798

Saha, S., Moorthi, S., Pan, H.-L., Wu, X., Wang, J., Nadiga, S., Tripp, P., Kistler, R., Woollen, J., Behringer, D., Liu, H., Stokes, D., Grumbine, R., Gayno, G., Wang, J., Hou, Y-T., Chuang, H-Y., Juang, H-M. H., Sela, J., Iredell, M., Treadon, R., Kleist, D., Van Delst, P., Keyser, D., Derber, J., Ek, M., Meng, J., Wei, H., Yang, R., Lord, S., Van Den Dool, H., Kumar, A., Wang, W., Long, C., Chelliah, M., Xue, Y., Huang, B., Schemm, J-K., Ebisuzaki, W., Lin, R., Xie, P., Chen, M., Zhou, S., Higgins, W., Zou, C-Z., Liu, Q., Chen, Y., Han, Y., Cucurull, L., Reynolds, R. W., Rutledge, G., & Goldberg, M. (2010). The NCEP Climate Forecast System Reanalysis. *Bulletin of the American Meteorological Society*, *91*(8), 1015–1057. http://doi.org/10.1175/2010BAMS3001.1

Schodlok, M. P., Menemenlis, D., Rignot, E., & Studinger, M. (2012). Sensitivity of the ice-shelf/ocean system to the sub-ice-shelf cavity shape measured by NASA IceBridge in Pine Island Glacier, West Antarctica. *Annals of Glaciology*, *53*(60), 156–162. http://doi.org/10.3189/2012AoG60A073

Smith, S. D. (1988). Coefficients for Sea Surface Wind Stress, Heat Flux, and Wind Profiles as a Function of Wind Speed and Temperature. *Journal of Geophysical Research: Oceans*, *93*(88), 467–472.

Stull, R. (1988). An Introduction to Boundary Layer Meteorology. Dordretch; London: Kluwer Academic Publishers.

Suortti, T. M., Kivi, R., Kats, A., Yushkov, V., Kampfer, N., Leiterer, U., Miloshevich, L. M., Neuber, R., Paukkunen, A., Ruppert, P., & Vomel. (2008). Tropospheric Comparisons of Våisålå Radiosondes and Balloon-Borne Frost-Point and Lyman-α Hygrometers during the LAUTLOS-WAVVAP Experiment. *Journal of Atmospheric and Oceanic Technology*, *25*, 149-166.

Thoma, M., Jenkins, A., Holland, D., & Jacobs, S. (2008). Modelling Circumpolar Deep Water intrusions on the Amundsen Sea continental shelf, Antarctica. *Geophysical Research Letters*, *35*(18), L18602. http://doi.org/10.1029/2008GL034939

Timmermann, R., Wang, Q., & Hellmer, H. H. (2012). Ice-shelf basal melting in a global finite-element sea-ice/ice-shelf/ocean model. *Annals of Glaciology*, *53*(60), 303–314. http://doi.org/10.3189/2012AoG60A156

Turner, J., Chenoli, S. N., abu Samah, A., Marshall, G., Phillips, T., & Orr, A. (2009). Strong wind events in the Antarctic. *Journal of Geophysical Research*, *114*, D18103. http://doi.org/10.1029/2008JD011642

Turner, J., Phillips, T., Hosking, J. S., Marshall, G. J., & Orr, A. (2013). The Amundsen Sea low. *International Journal of Climatology*, *33*(7), 1818–1829. http://doi.org/10.1002/joc.3558

Table 1. The latitude, longitude, altitude, mean temperature and mean pressure recorded at each of the four AWS: Evans Knoll (EK), Thurston Island (TI), Bear Peninsula (BP) and New York University (NYU).

Site Details	EK	TI	BP	NYU
Longitude (°W)	100.40	97.55	111.89	100.71
Latitude (°S)	74.85	72.53	74.55	75.01
Altitude (m)	178	212	312	70
Mean temp (°C)	-13.01	-11.21	-13.60	-15.39
Mean pressure (hPa)	962.7	954.4	930.3	975.3

Table 2. A comparison of 2-m temperatures from reanalyses to observed AWS temperatures. A negative bias indicates that the reanalysis product is colder than the observations. SON, DJF, MAM and JJA indicate the season. The standard deviation ratio (SD ratio) is the standard deviation of the reanalyses divided by that observed. R^2 has its standard statistical meaning as a measure of the correlation. RMSE is the Root Mean Square Error. Slope indicates the gradient of the linear regression line. The unit for bias and RMSE is °C. The AMRC site average is calculated from the Evans Knoll, Thurston Island and Bear Peninsula AWS sites. The right hand column shows the weighted mean annual bias across the four sites. *The NYU data set only covers a 13-month period.

Product	Stats	AMRC 3 site average				NYU*				Annual Avg. Bias
		SON	DJF	MAM	JJA	SON	DJF	MAM	JJA	
ERA-I	Bias	-2.27	-0.23	-2.66	-3.70	1.35	0.36	3.02	2.83	-1.80
	SD Ratio	1.17	1.09	1.29	1.25	0.88	0.90	0.97	0.95	
	R^2	0.79	0.72	0.74	0.73	0.93	0.83	0.88	0.86	
	RMSE	4.37	2.22	5.16	6.34	2.83	2.06	4.44	4.32	
	Slope	1.04	0.93	1.12	1.07	0.85	0.82	0.91	0.89	
JRA-55	Bias	-2.82	-1.91	-3.40	-3.89	0.07	-0.18	1.74	1.55	-2.62
	SD Ratio	1.01	1.14	1.03	0.92	0.81	0.84	0.82	0.74	
	R^2	0.82	0.74	0.80	0.80	0.83	0.69	0.84	0.76	
	RMSE	4.17	2.88	4.68	5.29	3.74	2.70	4.24	4.77	
	Slope	0.91	0.98	0.92	0.82	0.74	0.70	0.75	0.64	
CFSR	Bias	-2.88	-2.63	-2.96	-2.68	-0.48	-2.50	1.52	1.79	-2.50
	SD Ratio	1.20	1.37	1.26	1.18	1.04	1.29	1.00	1.06	
	R^2	0.75	0.62	0.75	0.73	0.78	0.59	0.84	0.79	
	RMSE	5.02	4.02	5.19	5.45	4.31	4.75	4.13	4.71	
	Slope	1.04	1.08	1.09	1.01	0.92	0.99	0.92	0.94	
MERRA	Bias	-6.62	-6.86	-7.87	-6.89	-4.57	-6.00	-4.21	-3.11	-6.80
	SD Ratio	1.06	1.28	1.12	0.99	0.95	1.04	1.01	0.98	
	R^2	0.82	0.73	0.79	0.80	0.85	0.75	0.83	0.81	
	RMSE	7.31	7.29	8.57	7.72	5.69	6.52	5.78	4.94	
	Slope	0.96	1.09	1.00	0.89	0.88	0.90	0.92	0.88	

Table 3. A comparison of the four reanalysis products across the four AWS sites for wind speed, relative humidity and specific humidity average over all seasons. The statistics are the same as those in Table 2. Note humidity is not available at the NYU site.

Product	Stats	wind speed (m s^{-1})		relative humidity (%)	specific humidity (g kg^{-1})
		AMRC	NYU	AMRC	AMRC
ERA-I	Bias	-1.32	-0.80	-5.20	-0.20
	SD Ratio	0.53	0.72	0.87	1.06
	R^2	0.43	0.63	0.25	0.87
	RMSE	5.73	3.22	14.12	0.39
	Slope	0.34	0.57	0.43	0.99
JRA-55	Bias	-0.58	-0.63	5.46	-0.25
	SD Ratio	0.61	0.81	0.66	1.03
	R^2	0.46	0.75	0.36	0.81
	RMSE	5.31	2.66	12.99	0.47
	Slope	0.42	0.70	0.37	0.92
CFSR	Bias	-1.85	-2.27	12.33	-0.05
	SD Ratio	0.54	0.57	0.47	1.12
	R^2	0.45	0.71	0.27	0.85
	RMSE	5.46	3.83	17.22	0.38
	Slope	0.36	0.48	0.23	1.04
MERRA	Bias	-0.40	-1.55		-0.63
	SD Ratio	0.43	0.68		0.74
	R^2	0.37	0.60		0.79
	RMSE	5.62	3.61		0.76
	Slope	0.32	0.53		0.65

Table 4. A comparison of the four reanalysis products to meteorological data from three research vessel cruises to the Amundsen Sea; *RRS James Clark Ross* (Feb 2014), the *Polarstern* (March 2010) and the *Palmer* (Jan-Feb 2009). Observational data are corrected from sensor height to reanalysis output height.

Product	Stats	pressure (hPa)	temp (°C)	wind speed (ms^{-1})	spec. Hum ($g\ kg^{-1}$)	rel. Hum (%)
ERA-I	Bias	0.00	-0.62	-0.82	-0.20	-3.73
	SD Ratio	1.00	1.20	0.97	1.08	1.03
	R^2	0.99	0.77	0.48	0.84	0.54
	RMSE	0.74	1.64	3.00	0.34	7.78
	Slope	1.00	1.04	0.67	0.99	0.77
JRA-55	Bias	-0.05	-0.39	-0.32	-0.03	2.03
	SD Ratio	1.01	1.22	0.96	1.11	0.84
	R^2	0.99	0.76	0.71	0.79	0.48
	RMSE	1.26	1.58	1.96	0.32	7.53
	Slope	1.00	1.04	0.81	0.97	0.59
CFSR	Bias	-0.22	-1.63	-0.83	-0.22	2.32
	SD Ratio	1.01	1.55	0.81	1.15	0.65
	R^2	0.97	0.72	0.46	0.83	0.34
	RMSE	1.85	2.88	2.88	0.39	8.66
	Slope	0.99	1.28	0.55	1.04	0.37
MERRA	Bias	0.46	-2.08	-1.02	-0.30	1.02
	SD Ratio	1.01	1.50	0.81	1.11	0.80
	R^2	0.98	0.60	0.62	0.71	0.26
	RMSE	1.46	3.38	2.46	0.51	9.10
	Slope	1.00	1.13	0.64	0.93	0.39

Table 5: Mean profile statistics from 975 hPa to 800 hPa for each of the reanalysis products for: temperature (Temp) (°C), relative humidity (%), specific humidity (g kg^{-1}) and wind speed (m s^{-1}). Along with the mean of all profiles (All), the profiles have been split into groups as follows: Shelf Break and Continental, Inversion and Non-Inversion, and Low Level Jet (LLJ) and Non-Low Level Jet (Non-LLJ). The number of soundings in each group is noted in column 2.

		ERA-I		**JRA-55**		**CFSR**		**MERRA**	
		Bias	RMSE	Bias	RMSE	Bias	RMSE	Bias	RMSE
temp	**All (38)**	**-0.54**	**1.42**	**-1.22**	**1.88**	**-0.79**	**1.96**	**-1.19**	**2.03**
	Shelf Break (11)	0.11	1.27	-0.28	1.21	0.47	1.68	-0.31	1.47
	Continental (27)	-0.80	1.46	-1.60	2.06	-1.29	2.06	-1.50	2.13
	Inversion (16)	-0.54	1.64	-1.64	2.26	-1.02	2.19	-1.52	2.18
	Non-inv (22)	-0.55	1.21	-0.92	1.54	-0.62	1.77	-0.93	1.88
rel. Hum	**All**	**-1.22**	**12.47**	**-3.53**	**16.07**	**2.53**	**11.80**	**-7.67**	**17.59**
	Inversion (16)	-2.68	13.09	-3.96	15.48	2.03	11.59	-10.63	19.31
	Non-inv (22)	-0.16	11.82	-3.21	16.33	2.88	11.83	-5.48	15.98
spec. Hum	**All**	**-0.05**	**0.24**	**-0.16**	**0.33**	**-0.02**	**0.29**	**-0.23**	**0.38**
	Inversion (16)	-0.08	0.26	-0.19	0.36	-0.05	0.24	-0.31	0.43
	Non-inv (22)	-0.02	0.22	-0.13	0.31	0.00	0.32	-0.17	0.32
wind speed	**All**	**-0.95**	**3.48**	**-1.22**	**3.40**	**-1.16**	**3.27**	**-0.75**	**3.30**
	LLJ (21)	-1.17	3.65	-1.75	3.67	-1.75	3.40	-1.26	3.55
	Non-LLJ (17)	-0.61	3.18	-0.43	2.89	-0.29	3.03	-0.01	2.85

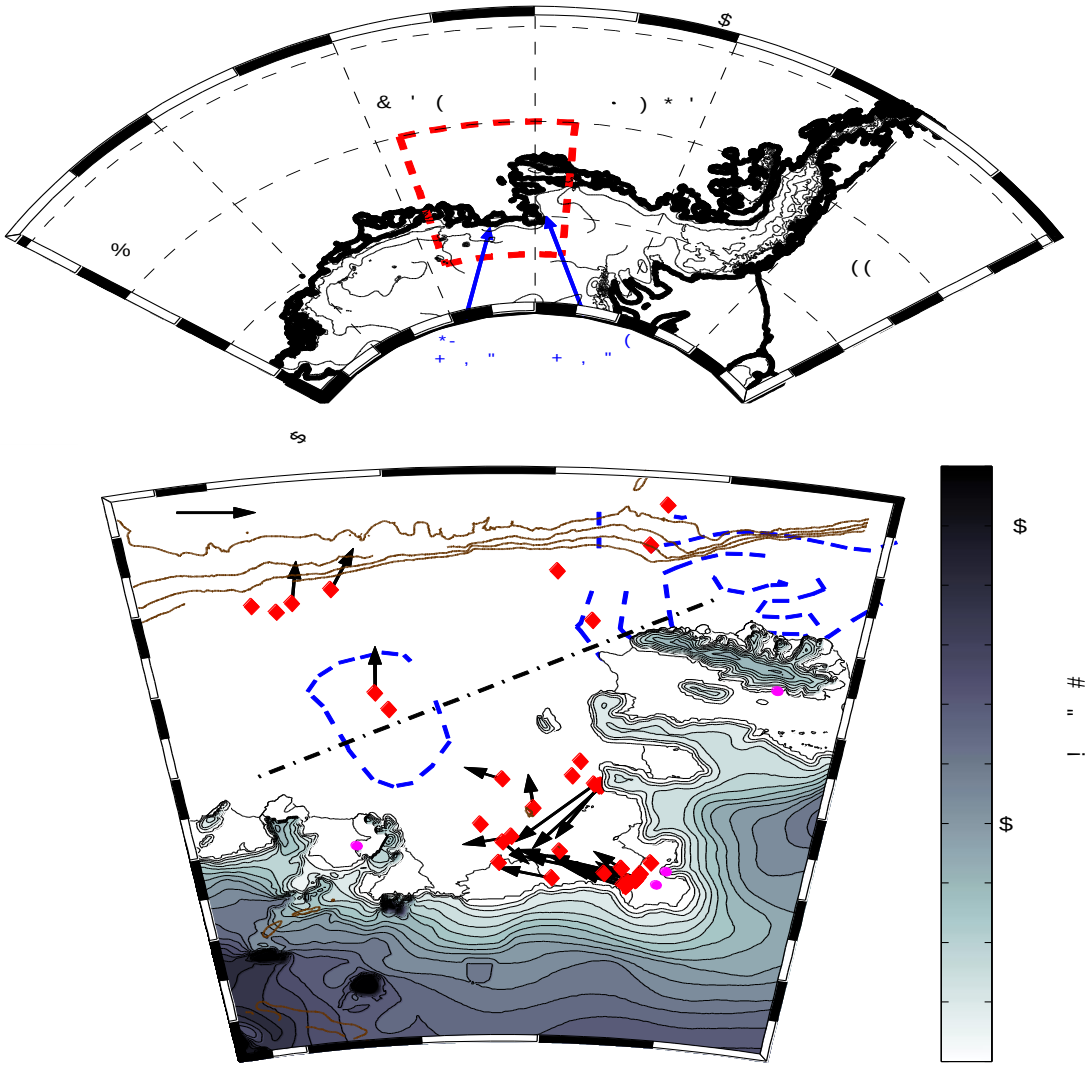

Figure 1. **(top)** West Antarctica with topographic contours every 500m and relevant seas and glaciers labelled. The red box outlines the area shown below. **(bottom)** Map of the Amundsen Sea Embayment (ASE), with topographic contours every 100m. The brown contour lines show bathymetry, the sharp slope marking the continental shelf break. The dashed blue lines shows the ERA-I mean sea-ice concentration during February 2014 when the radiosonde and JCR observations occurred. The red diamonds show the locations of the 38 radiosondes launched. The magenta circles show the locations of the four AWS sites, Bear Peninsula (BP), Evans Knoll (EK), Thurston Island (TI) and New York University (NY). The diagonal dashed black line indicates an arbitrary divide between continental and shelf break radiosondes. The vectors show the direction and relative strengths of low-level jets where they were observed in radiosonde profiles. The topographic data are grid cell average 2-minute elevation data from the Etopo2 version 2 NOAA database, derived from the GLOBE digital elevation model.

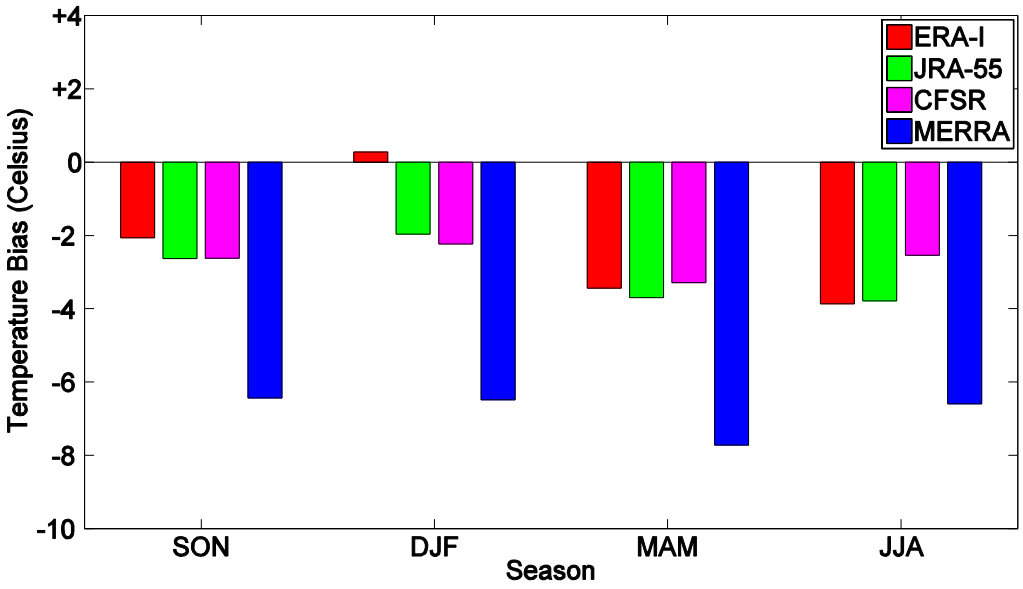

Figure 2. The magnitude of seasonal temperature biases for each of the reanalysis products at the Bear Peninsula AWS.

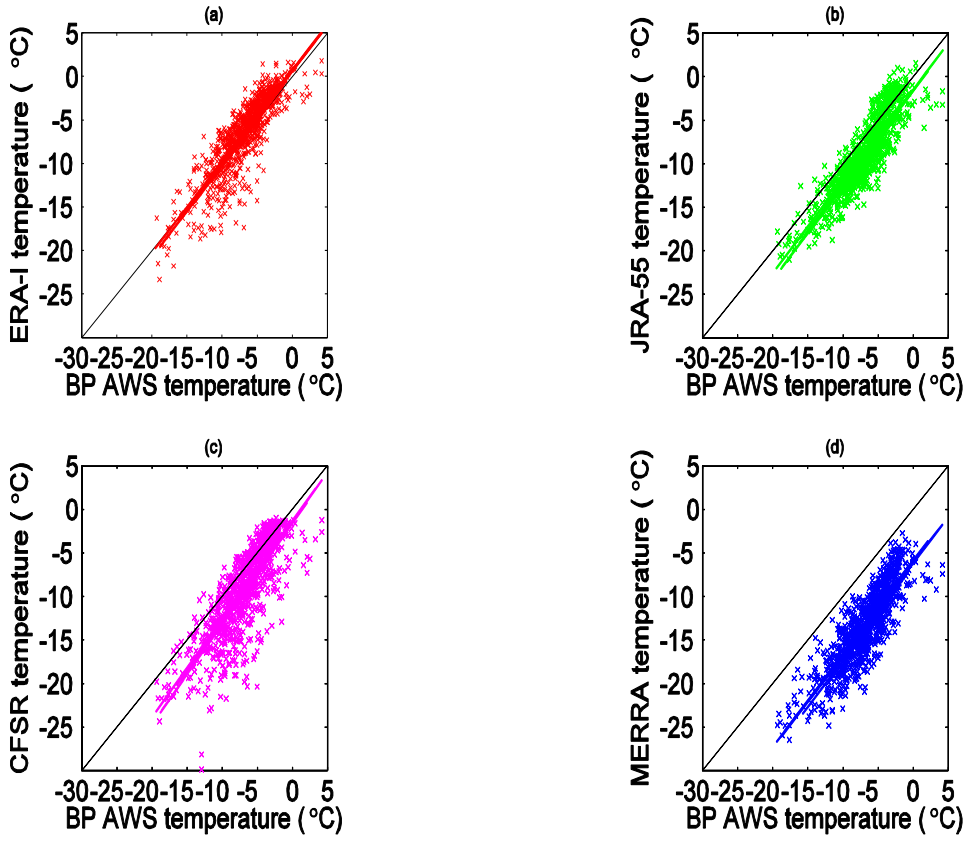

Figure 3. Scatter plots showing the Bear Peninsula (BP) AWS observed summertime temperature (2011-2014) against the 2-m temperatures from the reanalyses: **(a)** ERA-I, **(b)** JRA-55, **(c)** CFSR and **(d)** MERRA.

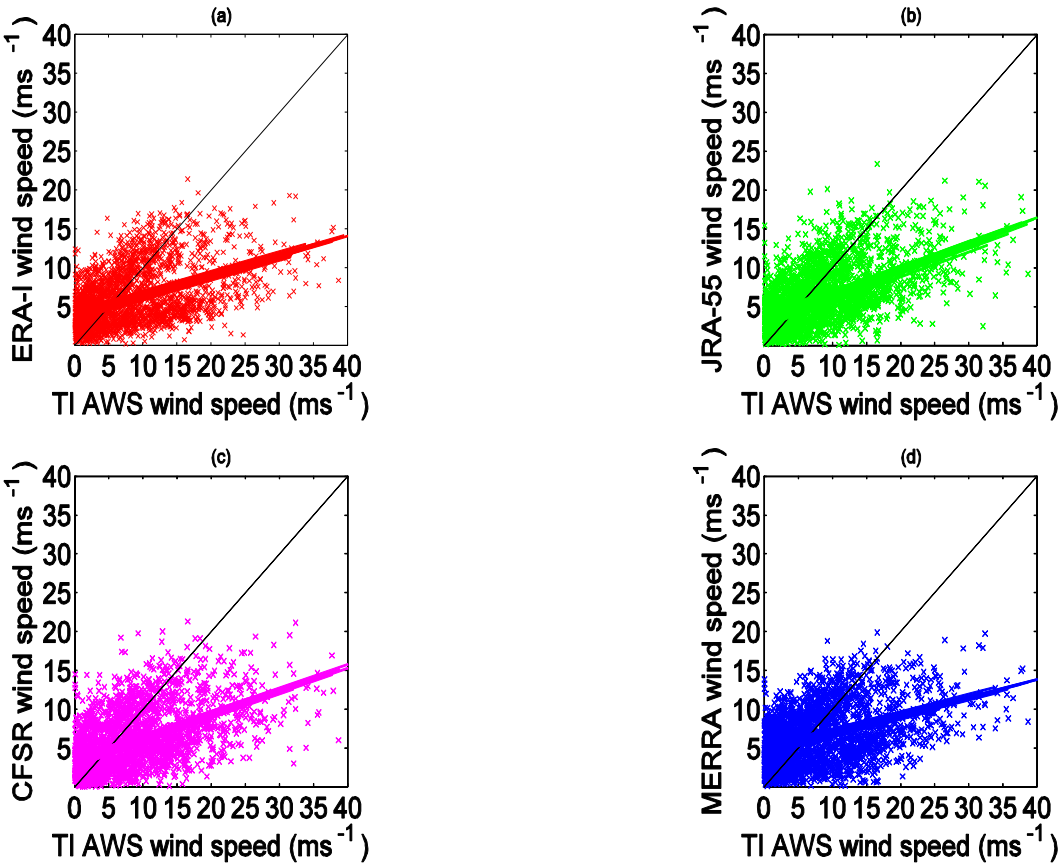

Figure 4. Scatter plots showing the Thurston Island (TI) AWS observed wind speed (2011-2014) against the neutrally adjusted 3m wind speed from the reanalyses: **(a)** ERA-I, **(b)** JRA-55, **(c)** CFSR and **(d)** MERRA.

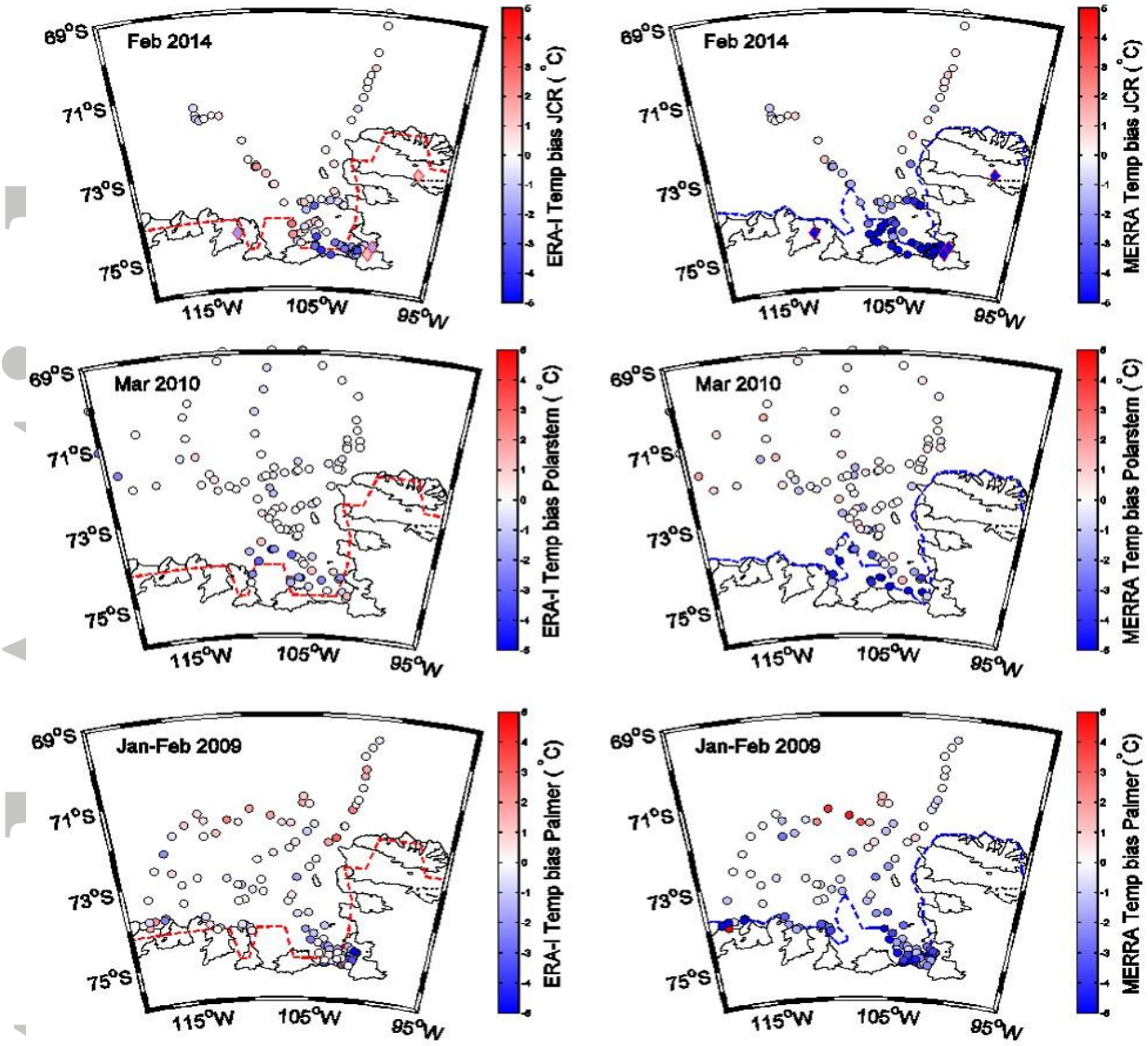

Figure 5: Spatial variability of reanalysis temperature biases **(ERA-I left column**, **MERRA right column)** in comparison to ship meteorological data from: *RRS JCR* **(top row)**, the *Polarstern* **(middle row)**, and *Palmer* **(bottom row)**. In the *JCR* figures the mean temperature bias from AWS for the month of Feb 2014 are shown in the diamonds with red edge colour. The dashed lines show the land sea mask (here the 0.95 contour is shown for ERA-I and 0.5 contour for MERRA).

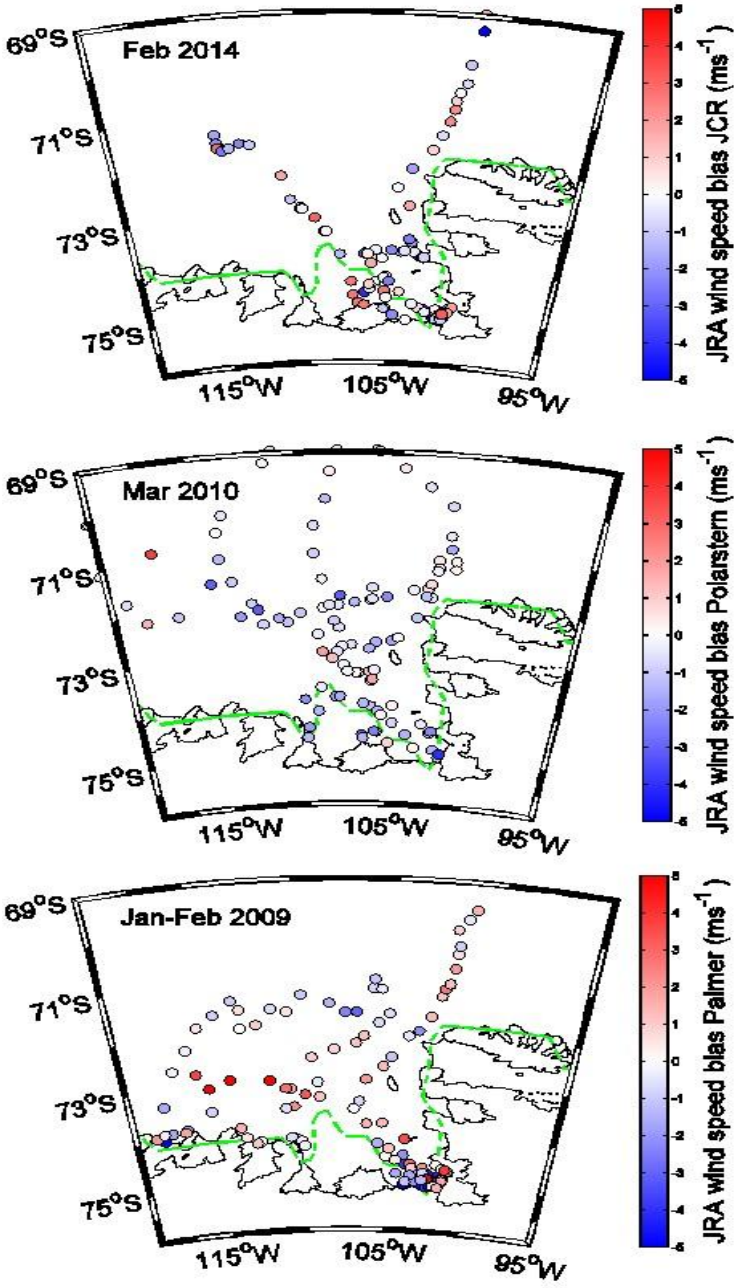

Figure 6: Spatial variability of wind speed biases for JRA-55 in comparison to ship meteorological data from: *RRS JCR* **(top)**, the *Polarstern* **(middle)**, and *Palmer* **(bottom)**. The dashed lines show land sea mask in each of the products (here the 0.5 contour is shown for JRA-55).

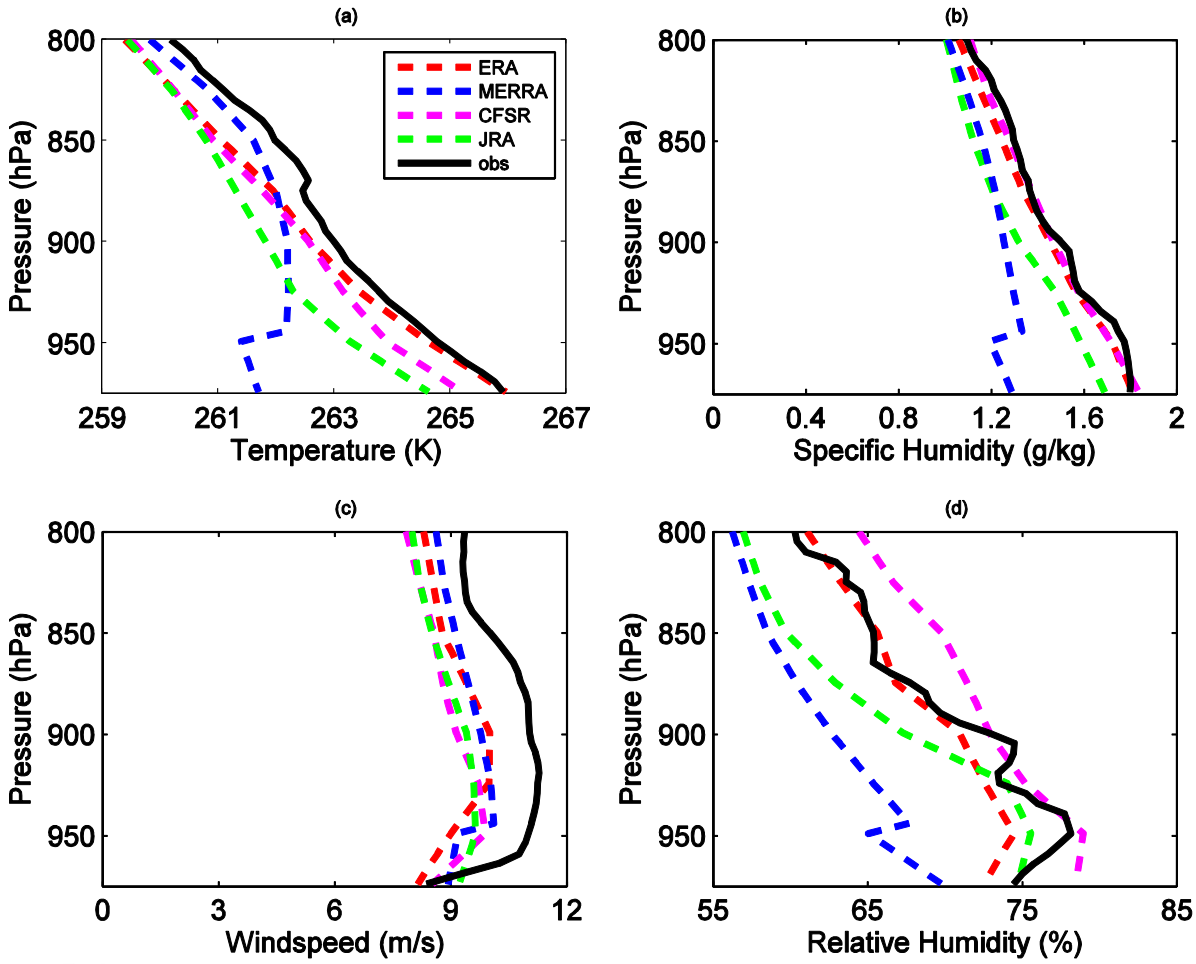

Figure 7. Mean atmospheric profiles from the radiosondes (1 Feb 2014 to 4 Mar 2014) and reanalyses: **(a)** temperature, **(b)** specific humidity, **(c)** wind speed, **(d)** relative humidity. The coloured lines represent the same reanalysis products as in figure 2: red ERA-I, green JRA-55, magenta CFSR and blue MERRA. Radiosonde observations are shown by the black line.

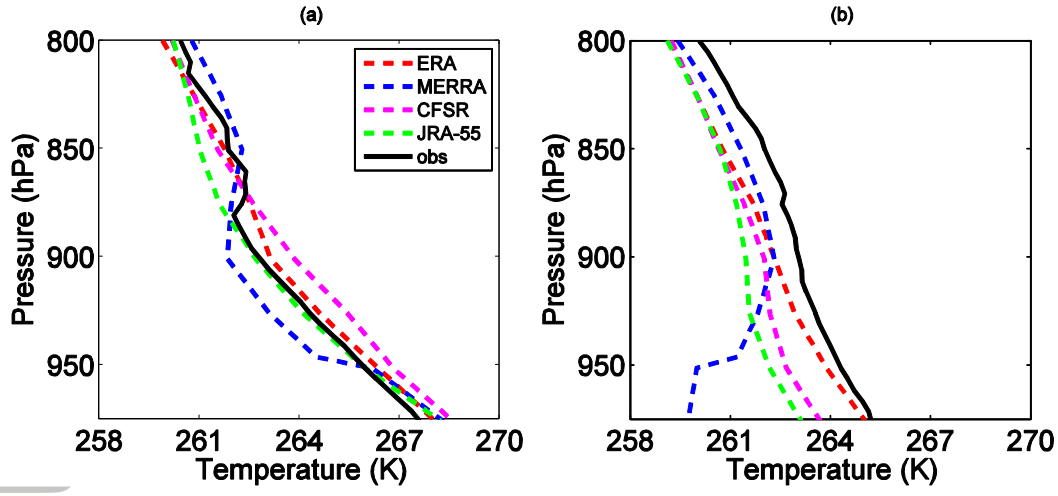

Figure 8. Radiosonde profile comparison split into two groups; **(a)** shelf break radiosondes (11 profiles), **(b)** continental radiosondes (27 profiles). The map in Fig. 1b shows the spatial split. The coloured lines represent the same reanalysis products as in Fig. 7.

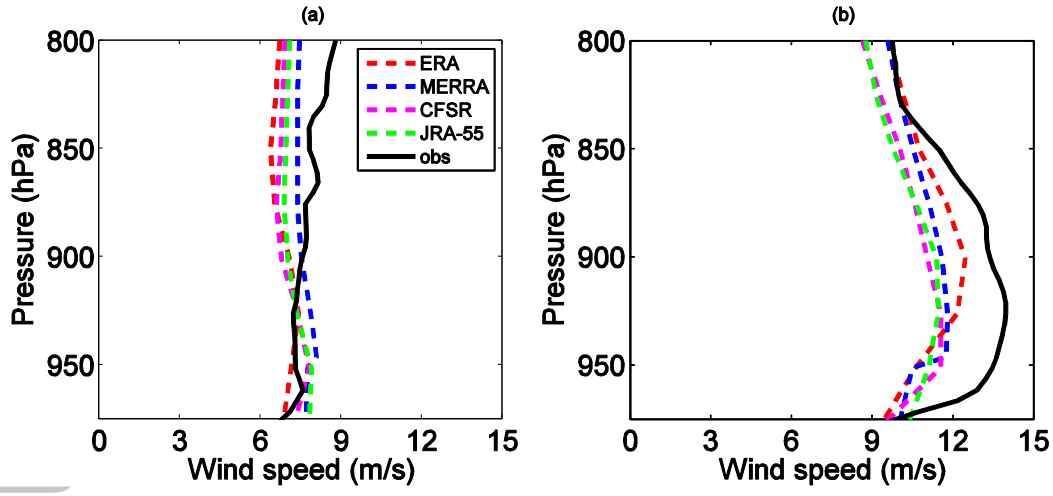

Figure 9. Average wind speed profiles split for two groups of radiosondes; (a) 17 profiles where a low level jet (LLJ) was not observed, (b) 21 profiles where a LLJ was recorded by the radiosonde. The coloured lines represent the same reanalysis products as in Fig. 7.